Molecular Cell
Article

The Acidic Transcription Activator Gcn4 Binds the Mediator Subunit Gal11/Med15 Using a Simple Protein Interface Forming a Fuzzy Complex

Peter S. Brzovic,[2,5] Clemens C. Heikaus,[1,2,5] Leonid Kisselev,[1] Robert Vernon,[2] Eric Herbig,[1,3] Derek Pacheco,[1] Linda Warfield,[1] Peter Littlefield,[2] David Baker,[2,4] Rachel E. Klevit,[2,*] and Steven Hahn[1,*]
[1]Division of Basic Sciences, Fred Hutchinson Cancer Research Center, Seattle, WA 98109, USA
[2]Department of Biochemistry
[3]Molecular and Cellular Biology Graduate Program
[4]Howard Hughes Medical Institute
University of Washington, Seattle, WA 98195, USA
[5]These authors contributed equally to this work
*Correspondence: klevit@u.washington.edu (R.E.K.), shahn@fhcrc.org (S.H.)
DOI 10.1016/j.molcel.2011.11.008

SUMMARY

The structural basis for binding of the acidic transcription activator Gcn4 and one activator-binding domain of the Mediator subunit Gal11/Med15 was examined by NMR. Gal11 activator-binding domain 1 has a four-helix fold with a small shallow hydrophobic cleft at its center. In the bound complex, eight residues of Gcn4 adopt a helical conformation, allowing three Gcn4 aromatic/aliphatic residues to insert into the Gal11 cleft. The protein-protein interface is dynamic and surprisingly simple, involving only hydrophobic interactions. This allows Gcn4 to bind Gal11 in multiple conformations and orientations, an example of a "fuzzy" complex, where the Gcn4-Gal11 interface cannot be described by a single conformation. Gcn4 uses a similar mechanism to bind two other unrelated activator-binding domains. Functional studies in yeast show the importance of residues at the protein interface, define the minimal requirements for a functional activator, and suggest a mechanism by which activators bind to multiple unrelated targets.

INTRODUCTION

Activation of transcription is the endpoint of many signal transduction pathways controlling cell growth, development, and stress response. Most transcription activators enhance transcription by binding and recruiting coactivator complexes that directly interact with the transcription machinery (e.g., SAGA, TFIID, and Mediator) and/or function to remodel chromatin (e.g., SWI/SNF, p300, NuA4/Tip60, and SAGA) (Dyson and Wright, 2005; Ge et al., 2002; Green, 2005; Mittler et al., 2003; Prochasson et al., 2003; Stevens et al., 2002; Yang et al., 2004). In many instances, activation domains (ADs) interact with multiple unrelated coactivators. Likewise, coactivators can bind multiple and seemingly unrelated ADs. (Dames et al., 2002; Freedman et al., 2002, 2003; Herbig et al., 2010; Reeves and Hahn, 2005). What constitutes a functional AD and how these domains work with this apparent lack of binding specificity remains unclear.

Although not conserved in primary sequence (Martchenko et al., 2007), ADs often have a simple and biased sequence composition and are enriched for specific residue types, such as acidic residues, proline, or glutamine. Most known ADs are disordered in the absence of a binding target (Dyson and Wright, 2005). This property is not limited to ADs because many functional eukaryotic protein segments and, in some cases, entire proteins lack a stable tertiary structure (Dunker et al., 2001). There are many examples of disordered proteins whose structure is stabilized to different extents upon interaction with their binding partners (Dyson and Wright, 2005; Tompa and Fuxreiter, 2008).

Acidic ADs are an important class of activators that universally stimulate transcription in all eukaryotes tested (Ptashne and Gann, 2002). Originally recognized in yeast Gal4 and Gcn4 (Hope et al., 1988; Ma and Ptashne, 1987), the acidic activators encompass most of the well characterized yeast ADs and include strong mammalian and viral activators such as p53, E2F, and Vp16. P53 contains tandem ADs; several structures containing these domains, which are bound to coactivator targets, reveal binding via one or two short α helices. These interactions are mediated primarily by hydrophobic contacts and can be facilitated by charged and/or polar interactions (Di Lello et al., 2006; Feng et al., 2009; Kussie et al., 1996; Langlois et al., 2008; Uesugi et al., 1997). However, these known protein interfaces have a fairly specific geometry, and the general basis for how activators and their targets can bind multiple unrelated partners is not understood.

Yeast Gcn4, which contains tandem acidic ADs (Figure 1A) that act in conjunction with the coactivators Mediator, SAGA, and SWI/SNF (Brown et al., 2001; Fishburn et al., 2005; Herbig et al., 2010; Jedidi et al., 2010; Swanson et al., 2003; Yoon et al., 2003), directly regulates >70 genes involved in diverse

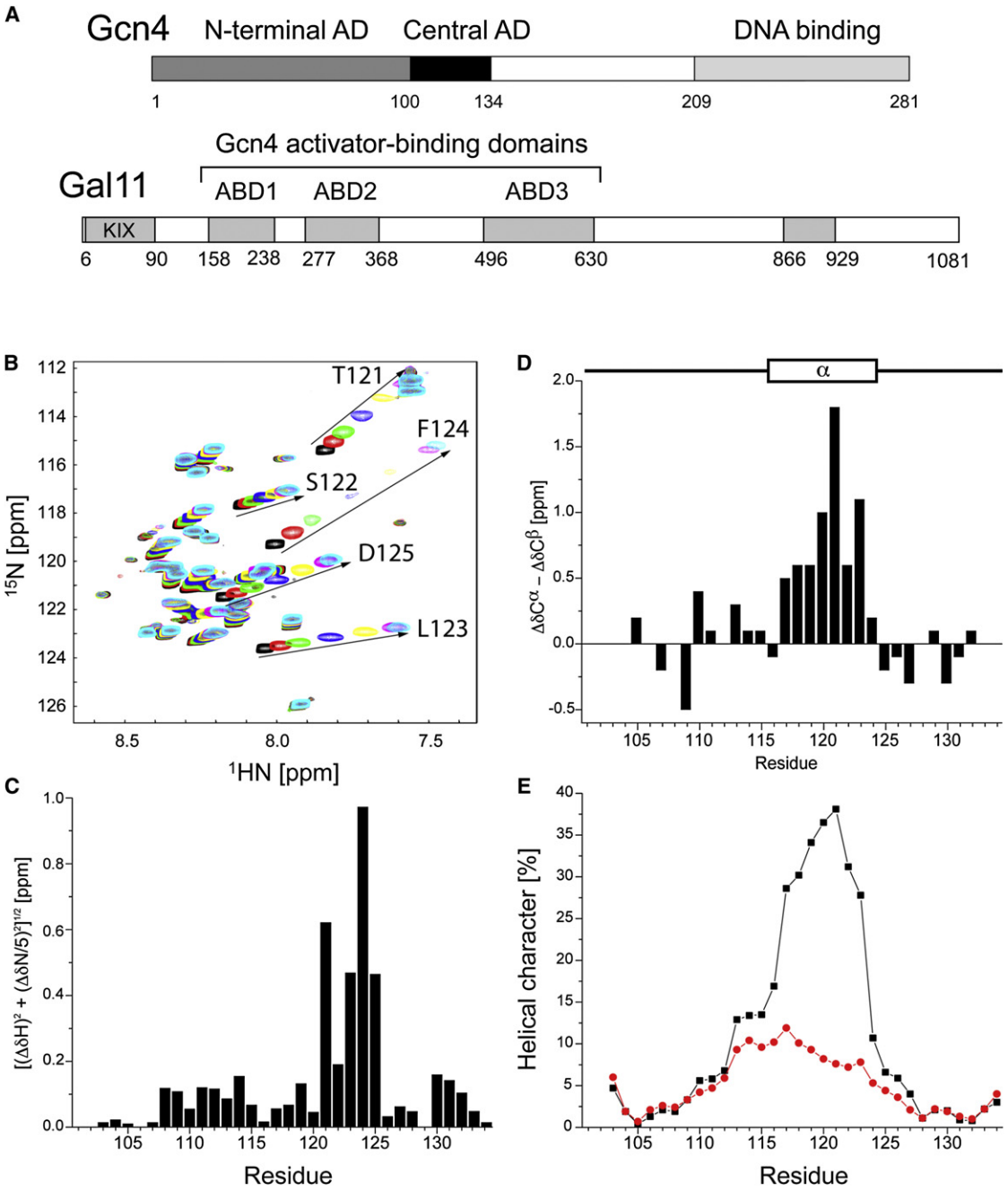

Figure 1. Gcn4 cAD Forms a Short α-Helix upon Binding to Gal11

(A) Position of the two Gcn4 ADs and three Gal11 domains (ABD-1, -2, -3) that bind Gcn4. Conserved regions of Gal11 are shown in gray.

(B) $^{1}H,^{15}N$-HSQC spectra of 0.3 mM ^{15}N-labeled Gcn4 (101–134) in the absence (black) and presence of 0.125 (red), 0.25 (green), 0.5 (blue), 1 (yellow), 2 (magenta), or 3 equivalents (cyan) of Gal11 ABD1 (158–238). Amides with the largest chemical shift perturbations (residues 121–125) are labeled and highlighted by arrows.

(C) Backbone amide chemical-shift perturbations of Gcn4 upon addition of 3 equivalents of ABD1. The formula $[(\Delta\delta H)^2\text{-}(\Delta\delta N/5)^2]^{1/2}$ was used to calculate the combined chemical shifts of ^{15}N and $^{1}H^{N}$. No $^{1}H^{N}$-peaks were observed for residues 101 and 102.

(D) Combined chemical-shift perturbations of $^{13}C^{\alpha}$ and $^{13}C^{\beta}$ of Gcn4 (101–134) bound to ABD1 in reference to free Gcn4. The location of the cAD α-helix is indicated.

(E) Probability for the formation of α-helical secondary structure elements predicted by CS-Rosetta (Shen et al., 2008) for Gcn4 (101–134) in the absence (red) and presence (black) of ABD1. NMR chemical-shift assignments of $^{13}C^{\alpha}$, $^{13}C^{\beta}$, $^{13}C'$, ^{15}N, and $^{1}H^{N}$ for free and bound Gcn4 were input and used for the generation of 100 9-residue fragments starting at each residue. The percentage of fragments showing helical secondary structure at each position is shown.

See also Figure S1.

processes, such as the response to metabolic stress and autophagy. The two Gcn4 ADs (residues 1–100 and 101–134) are unrelated in sequence apart from their acidic character. Site-specific crosslinkers that are positioned within either of the Gcn4 ADs and incorporated into pre-initiation complexes (PICs) target three common coactivator subunits: Gal11/Med15 (Mediator), Tra1 (SAGA and NuA4), and Taf12 (TFIID and SAGA) (Fishburn et al., 2005; Herbig et al., 2010), whereas full-length Gcn4 also binds two subunits of the chromatin remodeler SWI/SNF (Prochasson et al., 2003). Gal11 has three conserved Gcn4-binding domains (Figure 1A) that bind Gcn4 with micromolar affinity (Herbig et al., 2010; Jedidi et al., 2010; Majmudar et al., 2009; Park et al., 2000). These multiple, weak Gcn4-Gal11 interactions additively contribute to overall transcription activation and illustrate an important principal of Gal11 recruitment by Gcn4: Gcn4 binds Gal11 not by a single high-affinity and high-specificity interacton but rather by multiple low-affinity interactions.

To understand the molecular basis for Gcn4-Gal11 complex formation and to investigate principles that govern how activators and their targets bind multiple unrelated partners, we examined the structure and function of a representative Gcn4-Gal11 complex. We find that the Gcn4 AD adopts a helical conformation upon binding Gal11. Complex formation is driven primarily by relatively weak hydrophobic protein contacts that allow Gcn4 to bind Gal11 in multiple orientations. These findings and the accompanying functional studies suggest a mechanism for how activator-binding domains recognize seemingly unrelated activators and further define the minimal requirements for a functional AD.

RESULTS

The Gcn4 Tandem Activation Domains Are Intrinsically Disordered and Structurally Independent

The structural properties of the Gcn4 tandem ADs were investigated using nuclear magnetic resonance (NMR) spectroscopy. The $^{1}H,^{15}N$-HSQC spectra of each individual AD (Gcn4 1–100 and 101–134) overlaid almost perfectly with the spectrum of a construct containing both ADs (residues 1–134), indicating that the two regions are structurally independent (Figure S1A). In all three spectra, the resonances are dispersed over a narrow range in the $^{1}H^{N}$-dimension, indicating that both Gcn4 ADs are intrinsically disordered in the absence of binding partners. Our observation of a lack of ordered secondary structure is consistent with a previous NMR analysis of a Gcn4 fusion protein containing residues 39–139 (Huth et al., 1997). Based on its smaller size, the 34-residue central AD (cAD) of Gcn4 was chosen for further structural characterization of its interactions with Gal11. Backbone ^{13}C, ^{15}N, and $^{1}H^{N}$ NMR resonances of the cAD (residues 101–134; Figure 1A) were assigned using conventional heteronuclear techniques (Sattler et al., 1999). Backbone resonance chemical shifts, particularly $^{1}H^{\alpha}$, $^{13}C^{\alpha}$, and $^{13}C^{\beta}$ shifts, depend on local backbone geometry and provide a means to identify regions of regular secondary structure (Wishart et al., 1991). Consistent with a lack of ordered secondary structure, no patterns could be discerned from the cAD chemical shifts.

The Gcn4 Central AD Adopts a Helical Conformation upon Binding to Gal11-158–238

Binding of the cAD to the first Gal11 activator-binding domain (ABD1, residues 158–238) (Herbig et al., 2010) was monitored by collecting a series of ^{1}H, ^{15}N-HSQC spectra of ^{15}N-labeled cAD mixed with increasing concentrations of ABD1 (Figure 1B). Several cAD backbone amide resonances were strongly perturbed upon addition of ABD1. At the endpoint of the NMR titration (3-fold molar excess of ABD1), perturbations of up to 1.0 ppm were observed for residues 121–125 (Figure 1C). Importantly, similar shifts were observed in the spectrum of the tandem Gcn4-ADs when Gcn4 1–134 was titrated with ABD1, suggesting that the mode and affinity of interaction between the cAD and ABD1 is conserved in the context of the tandem Gcn4 ADs (Figure S1B).

To further characterize the structural properties of Gal11-bound Gcn4, backbone and side-chain resonance assignments were determined for Gcn4-cAD in the presence of excess ABD1. Comparison of Gcn4 backbone resonances ($^{1}H^{N}$, ^{15}N, $^{13}C^{\alpha}$, $^{13}C^{\beta}$, and $^{13}C'$) in the free and bound states indicated that the cAD adopts an α-helical conformation for binding to ABD1. The difference in chemical shift between free cAD and CAD bound to ABD1 was calculated for each $^{13}C^{\alpha}$ ($\Delta\delta^{13}C^{\alpha}$) and $^{13}C^{\beta}$ ($\Delta\delta^{13}C^{\beta}$) resonance and combined ($\Delta\delta^{13}C^{\alpha}$–$\Delta\delta^{13}C^{\beta}$) to obtain a composite chemical shift difference for each residue (Figure 1D). The histogram showed a contiguous stretch of positive combined differences for residues S117–F124, strongly indicating α-helical structure (Marsh et al., 2006). In contrast, the combined carbon chemical shift differences of residues 103–116 and 125–134 were much smaller and showed no trends, indicating that these residues do not take on regular secondary structure in the bound state. $^{13}C'$ and $^{1}H^{\alpha}$ chemical-shift values also indicated stabilization of helical structure upon binding: $^{13}C'$ resonances of residues 115–122 shifted downfield upon addition of Gal11 (Figure S1C) and $^{1}H^{\alpha}$ resonances of residues 117–127 resonated upfield when compared to random-coil values (Figure S1D); the $^{1}H^{\alpha}$-chemical shifts for free Gcn4-cAD were not assigned.

The backbone resonance assignments of the free and bound states of the cAD were used as input for CS-ROSETTA, a protocol that uses NMR chemical shifts to predict protein structure (Shen et al., 2008, 2009). Up to 40% of the fragments generated by CS-ROSETTA exhibited helical character when the bound chemical-shift values were input (Figure 1E, black), whereas no significant helical character was predicted for free Gcn4-cAD (Figure 1E, red). The prediction of helical character is particularly high for residues S117–L123. Thus, chemical shift differences and CS-ROSETTA output indicate that Gcn4-cAD residues S117–F124 adopt a helical conformation upon binding to ABD1.

Structure of Gal11-ABD1

Backbone and side-chain resonance assignments for $^{13}C,^{15}N$-labeled ABD1 were determined in the presence of excess Gcn4-cAD. Nearly complete assignments (>98%) were obtained for the cAD in the presence of excess ABD1. Dihedral angle constraints were derived from backbone assignments using the program TALOS (Cornilescu et al., 1999). Distance

Table 1. Experimental NMR Restraints and Structural Statistics for the Gal11 Structure

Structural Restraints (Residues 158–238)		
NOE distance restraints	472	
Short-range (|i–j| = 1)	189	
Medium-range (|i<|i–j|<5)	98	
Long-range (|i–j|>5)	59	
NOE constraints per restrained residue	6	
Dihedral-angle constraints	132	
Restraint Violations		
Distance violations (per model)		
0.1–0.2Å	2.40	
0.2–0.5Å	0.05	
>0.5Å	0.00	
Dihedral-angle violations per model (1°–10°)	2.10	
Ensemble Rmsd (50 models)	All	Ordered
All backbone atoms	2.3Å	0.9Å
All heavy atoms	2.9Å	1.3Å
(ordered residues: 163–187, 191–193, 195–232)		
Ramachandran Statistics		
Most favored	92.2%	
Additionally favored	7.8%	
Generously allowed	0.0%	
Disallowed	0.0%	

NMR, nuclear magnetic resonance; NOE, nuclear overhauser effect; Rmsd, root mean square deviation.

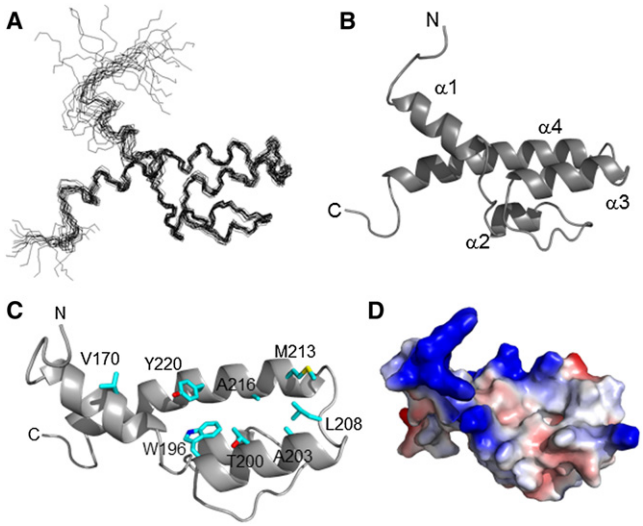

Figure 2. Solution Structure of Gal11-ABD1

(A) NMR ensemble of 20 low-energy Gal11-ABD1 structures. Average pairwise RMSDs for the ordered backbone atoms of residues 163–187, 191–193, 195–232 is 0.9Å.

(B) Ribbon representation of the Gal11-ABD1.

(C) Orientation from (A) was rotated ~90 degrees about the x-axis to highlight the residues from α1, α3, and α4 that form the ABD1 hydrophobic cleft (shown in stick representation with carbons in blue, oxygens in red, and sulfur in yellow).

(D) The surface electrostatic potential of ABD1 oriented as in (B). Red, negatively polarized; blue, positive; white, nonpolar.

restraints used for structure calculations were derived from analysis of aliphatic and aromatic ^{13}C-NOESY-HSQC and ^{13}C-edited, ^{13}C-filtered NOESY spectra (Table 1). These data were used first to calculate the structure of ABD1 (Figure 2A), which is comprised primarily of four α helices. A long 26-residue C-terminal helix, α4, spans the entire length of the domain; the remaining helices (α1, α2, and α3) are all oriented antiparallel with respect to α4 (Figure 2B). Helix α3 runs directly antiparallel to α4 and is linked to α4 via an extended 5-residue segment. Helix α1 is angled relative to the plane formed by helices α3 and α4. There is some minor variation in the angle of helix α1 because the restraints of the nuclear overhauser effect (NOE) were not sufficient to define a single orientation. The region between α1 and α3 (residues 175–195) covers one face of the α3-α4 plane. Mostly an extended structure, this segment includes the short α2 helix (residues 180–185). The α1, α3, and α4 helices create a cleft with a largely hydrophobic floor formed by residues W196 and Y220 and flanked by V170, T200, A203, L208, M213, and A216 (Figure 2C). The electrostatic surface of ABD1 has a net overall positive potential, and the hydrophobic cleft is bounded by a number of positively charged residues (Figure 2D). A 3D structure search using the DALI (Holm et al., 2008) and COPS servers (Suhrer et al., 2009) failed to identify any structural homologs, indicating that the Gal11-ABD1 structure represents a unique domain fold.

The Gcn4-Gal11 Interface

The ^{1}H,^{15}N-HSQC titration data are consistent with the binding of Gcn4-cAD to the ABD1 hydrophobic cleft but are not definitive because a large number of Gal11 resonances shift upon interaction with Gcn4 (Figures S1E and S1F). To examine the intermolecular interaction, we adopted a three-tiered approach involving: 1) analysis of intermolecular NOEs, 2) modification of the Gcn4-cAD with paramagnetic spin-labels, and 3) computational docking of Gcn4-cAD onto the Gal11-ABD1. As described below, the sum of these approaches shows that Gcn4 binds to the Gal11 hydrophobic cleft, although there is no single mode of interaction. Instead, the short Gcn4 helix binds in multiple orientations with respect to Gal11, a characteristic of intrinsically disordered proteins that form "fuzzy" complexes (Tompa and Fuxreiter, 2008).

^{13}C-edited and ^{13}C-edited, ^{13}C-filtered-NOESY spectra encompassing the aliphatic resonances of ABD1, were collected to identify intermolecular interactions. The ^{13}C-edited, ^{13}C-filtered-NOESY spectrum allows selective observation of magnetization transferred from the aliphatic side chains of ^{13}C-labeled ABD1 to protons on ^{12}C-labeled Gcn4-cAD. However, several features of the complex impact interpretation of the intermolecular NOE data: 1) the ABD1-cAD complex is in intermediate-to-fast exchange on the NMR time scale

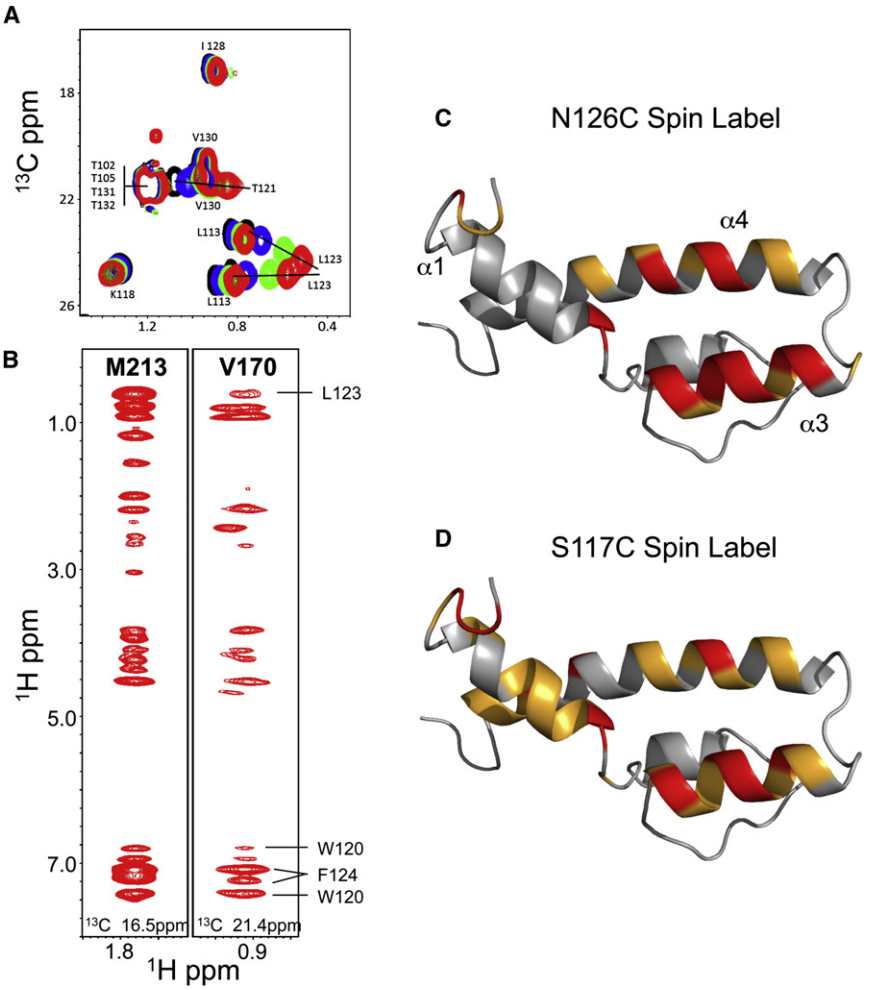

Figure 3. NMR Spectra of the Gal11-ABD1/Gcn4-cAD Complex and Effects of Gcn4 Paramagnetic Spin Labels

(A) Titration of ^{13}C-labeled Gcn4-cAD with unlabeled ABD1. The portion of the ^{1}H,^{13}C-HSQC shows the chemical shift perturbations of the T121 and L113 methyl groups upon binding to ABD1. The trajectories of these groups were used to assign resonances that arise from intermolecular interactions observed in NOESY spectra.

(B) Portions of the ^{13}C-edited, ^{13}C-filtered NOESY spectrum showing crosspeaks that arise from M213 and V170. Labeled crosspeaks could be unambiguously assigned to specific Gcn4 residues. M213 and V170 are located at opposite ends of the ABD1 hydrophobic cleft (Figure 2B), yet show crosspeaks to the same Gcn4 residues, suggesting that Gcn4 binds to ABD1 in multiple orientations.

(C and D) Paramagnetic spin labels were incorporated at four different positions of the cAD (104, 117, 126, 133), where positions 117 and 126 flank the nascent Gcn4-cAD helix. Observed intensity perturbations in ABD1 upon complex formation with Gcn4 spin-labeled at positions 126 and 117 are shown. Gal11 (gray ribbon), with strongly affected residues (intensity decrease > 80% relative to reference spectrum) in red and significantly affected residues (intensity decrease between 50%–80%) in orange.

See also Figure S2.

(Figure 1B), indicating a lifetime in the low millisecond range for the complex; 2) the cAD is present in excess and is unstructured in the unbound state; and 3) the molecular weights of the individual components and the protein complex are relatively small. Thus, multiple binding and dissociation events occur during the NOESY mixing time (140 ms) and the observed NOESY crosspeaks do not arise from a single static complex. These factors are often encountered in systems that give rise to transferred NOEs (Campbell and Sykes, 1993; Sykes, 1993). Therefore, the chemical shifts of crosspeaks corresponding to cAD resonances represent a weighted average of chemical shifts in the free and bound states. To properly interpret the spectra, we collected a series of ^{1}H,^{13}C-HSQC spectra of Gcn4-cAD at increasing concentrations of ABD1. The titrations define the trajectory of Gcn4 aliphatic and aromatic protons that shift upon complex formation. Figure 3A shows a representative section of the ^{1}H,^{13}C-HSQC aliphatic region. Substantial shifts are particularly evident for the Gcn4 methyl groups of L123 and T121, residues that adopt helical character upon binding to ABD1. Likewise, the aromatic resonances of Gcn4 W120 and F124 undergo large changes in chemical shift (Figure S2A). In contrast, the methyl resonances of L113 (Figure 3A) and the aromatic resonances of F108 and Y110 (Figure S2A) shift, but to a much smaller extent.

Examination of the NOESY spectra show that Gal11 residues L162, Q167, L169, V170, V199, T200, A203, M213, A216, K217, and Y220 are in NOE contact with Gcn4 residues W120, T121, L123, and F124. What is particularly striking is that side chains throughout the Gal11-ABD1 binding cleft interact with the same set of Gcn4 hydrophobic residues. For instance, both V170 and M213, which are located at opposite ends of the ABD1 hydrophobic cleft (Figure 2C), exhibit NOEs to same protons in the W120, T121, L123, and F124 side chains of Gcn4 (Figure 3B). These observations are consistent with a model in which the cAD binds to Gal11 in more than one orientation.

For the second tier of structural analysis, spin labels were attached to specific sites on the cAD. Single cysteine residues were introduced at four locations: residues 117 and 126, which flank the Gcn4 helical segment, and residues 104 and 133, which are located near the N- and C-termini of the Gcn4-cAD. Each cAD Cys-derivative was modified with the spin label 4C-(2-Iodoacetamido)-TEMPO. Spin-labeled cAD induces peak broadening of Gal11 resonances that are in proximity to the unpaired electron in TEMPO (Figure S2B; histograms of the residue-by-residue spin-label effects are shown in Figure S2C). The spin label at position 126 produces large decreases in peak intensity ($\geq$80%) in the Gal11 amide resonances of residues L162,

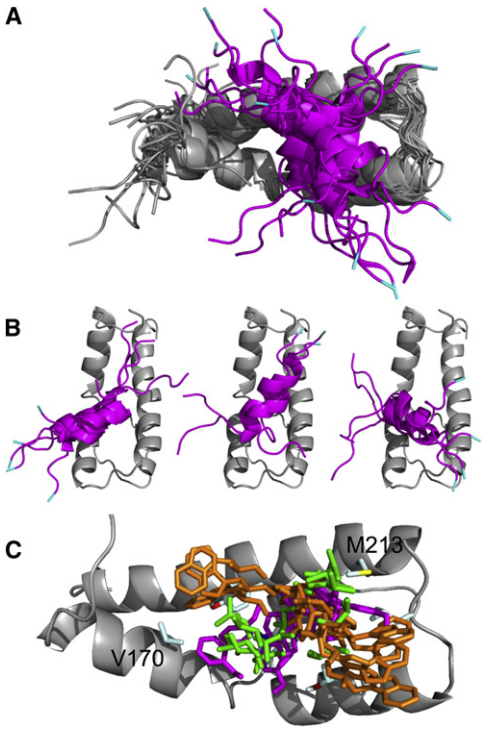

Figure 4. Models of the ABD1-cAD Complex Derived from NOE and Spin-Labeling Data

(A) Ribbon representations for the ensemble of HADDOCK generated structures for Gcn4-cAD (magenta) binding to the ABD1 (gray). Gcn4 residues 101-112 and 131-134 have been removed for clarity and L113 (cyan) marks the N-terminus.

(B) Three different orientations of the Gcn4 peptide are evident in the ensemble of structures depicted in (A).

(C) Positions of key Gcn4 side chains W120 (orange), L123 (green), and F124 (magenta) relative to ABD1 (gray ribbon) are shown from the ensemble in (A). ABD1 residues V170 and M213 are labeled. The different modes of binding bring W120, L123, and F124 in proximity to both residues, consistent with observations derived from the (^{13}C-edited, ^{13}C-filtered)-NOESY (see Figure 3B).

Q172, K174, W196, Q197, V199, T200, A201, A203, Q204, A216, K217, and Y220 (Figure 3C, red). These residues are located at the C-terminal end of α1 and helix α3 and at the N-terminal portion of α4. Smaller but significant effects on resonance intensity (50%–80% decrease) are observed in a second set of resonances, most of which are located on helix α4 in the region where it crosses helix α1 (Figure 3C, orange). Incorporation of a spin label at position 117 yielded similar results (Figure 3D). Resonances in α1 and α3 are affected by the spin label in this position, though to a lesser extent, whereas residues located in the region bounded by α1 and α4 and including the Gcn4-cAD N-terminal segment are perturbed to a greater extent (Figure S2C). Thus, placement of a spin label at either end of the Gcn4 helix affects residues throughout the hydrophobic binding cleft. In contrast, placement of spin labels near the cAD termini (residues 104 and 133) indicate that regions outside the cAD helix do not make close contact with ABD1. These spin-labeling experiments also support the model wherein the cAD binds to ABD1 in multiple orientations.

The finding that there is no single mode of interaction between the cAD and ABD1 precludes the determination of pairwise distance restraints to define the complex. The transferred NOEs observed in ^{13}C-edited, filtered ^{13}C-NOESY spectra do define Gal11 residues involved in complex formation. Therefore, during the third tier of structural analysis we used ambiguous interaction restraints (AIRs) to calculate models of the complex. AIRs allow for any interacting Gcn4 residue to potentially contact any Gal11 residue located at the intermolecular interface (Dominguez et al., 2003). Because Gcn4 adopts helical character upon binding Gal11, loose dihedral angle constraints were generated for the bound form of the Gcn4-cAD, using the program TALOS (Cornilescu et al., 1999). These constraints were used to create a starting ensemble of cAD structures with helical character and, together with the ensemble of ADB1 structures previously calculated, were used as starting structures to perform docking calculations with the program HADDOCK (Dominguez et al., 2003). We also included dihedral angle constraints and the unambiguous distance constraints used for the calculations of the ABD1 structure. The ABD1 domain (residues 169–232) was aligned in the resulting ensemble of 200 structures. The structures were filtered to select those most consistent with the spin-labeling data by requiring the presence of both S117 and N126 within 15–17Å of amides maximally affected (>80%) by spin labels at these positions. The 12 resulting structures are shown in Figure 4A. Examination of the complexes reveals three different orientations of the Gcn4 helix on ABD1 (Figure 4B). These three clusters are representative of Gcn4 binding but are not meant to be exclusive.

In each of the clusters, the hydrophobic face formed by Gcn4 residues W120, T121, L123, and F124 binds to the ABD1 hydrophobic cleft (Figure 4C). There is a shallow depression in the ABD1 surface located between helices α3 and α4, bounded by A203, L208, and M213 on one side, Y220 on the other; A216 and W196 is partly accessible, forming the base (Figures 2C and 2D). Typically, the aromatic side chain of either Gcn4 W120 or F124 inserts into this depression. In most models, these interactions position the nascent Gcn4 helix across the ABD1 α3 and α4 helices. Although the angle of intersection can range from nearly perpendicular to almost parallel, most models orient the helix in a way that can bring Gcn4 L123 in proximity to either Gal11 M213 or V170 (Figure 4C).

Importance of Residues at the Gcn4-Gal11 Interface

Alanine substitutions were made at Gcn4-cAD W120 and F124, with the residues making direct contact with Gal11-ABD1, Gal11 W196 positioned in the center of the activator-binding cleft, and Gal11 residues M213 and T200 located at the edge of the binding cleft. Binding affinities were measured using isothermal titration calorimetry (Table 2 and Figures S3A–S3E). Wild-type cAD binds ABD1 with a K_d of 10.1 μM, similar to values measured using fluorescence polarization (Herbig et al., 2010). As expected from NMR analysis, Ala substitutions at Gcn4 120 or 124 decreased binding affinity for ABD1 by 5.6- and 6.5-fold, respectively.

The Gal11-ABD1 W196 mutant did not bind the cAD. Circular dichroism spectra showed that this mutation disrupts ABD1 secondary structure with a significant decrease in α-helical

Table 2. Mutations within the Gcn4-Gal11 Interface Decrease the Affinity of interaction

Gal11	Gcn4 AD	K_d (μM)	ΔH (cal/mol)	ΔS (cal/mol/deg)
158–238	101–134	10.1 ± 1.4	−5394 ± 150	4.58
158–238	101–134 W120A	56 ± 6	−1823 ± 80	13.3
158–238	101–134 F124A	65 ± 3	−3880 ± 46	6.02
158–238 W196A	101–134	NM	NM	NM
158–238 M213A	101–134	76 ± 5	−2812 ± 78	9.32
158–238 T200A	101–134	10.5 ± 0.5	−5021 ± 62	5.81

Affinities were measured by ITC. NM, no measureable binding. See also Figure S3.

content (Figure S3F). As W196 lies at the intersection of three Gal11 α helices, it makes important contacts within the core of the domain and likely promotes cooperative folding in addition to forming part of the Gcn4-binding cleft. Mutation of Gal11 M213 to Ala decreased binding 7.5-fold without affecting the helical content of ABD1 (Figure S3F). However, the M213 side chain does contribute to the overall thermal stability of ABD1 because the melting temperature of this derivative decreased from 53° to 41° (data not shown). In contrast, Gal11 T200A showed no change in Gcn4 binding affinity. Given the hydrophobic nature of the interaction, it is likely that loss of polar character in moving from Thr to Ala has no significant effect.

To determine the effect of Gcn4 mutations on transcription activation in vivo, a series of mutations were generated in a Gcn4 derivative lacking a functional N-terminal AD and assayed for function in a yeast strain wherein Gal11 430–680 was deleted, leaving ABD1 as the highest affinity Gcn4 binding site (Herbig et al., 2010). Cells were grown under starvation conditions to induce Gcn4 expression and mRNA levels from three genes dependent on Gal11 and Gcn4 were measured by RT-qPCR (Figure 5). Two complications are encountered when measuring the in vivo effects of the Gcn4 mutants. First, activation by Gcn4 requires that ADs directly interact with Gal11 (Mediator), as well as Tra1 (SAGA/NuA4) and possibly SWI/SNF; therefore, this assay does not strictly measure Gcn4 interaction with Gal11. Second, the stability of Gcn4 is directly related to its role in activation because it is targeted for ubiquitylation and degradation while stimulating transcription (Hinnebusch, 2005; Irniger and Braus, 2003). Even under starvation-induced conditions, Gcn4 is normally unstable and present at very low levels. However, nearly all of the Gcn4 mutations used here show significantly elevated protein levels compared with the wild-type central AD (Figure S4A). Thus, the observed effects of these mutations on transcription activation may be partially obscured due to the elevated levels of these Gcn4 derivatives.

Under these conditions, deletion of Gcn4 reduced transcription ≥ 4-fold from all three genes. A triple Ala substitution of three Gcn4 hydrophobic residues at the Gal11 interface (120, 123, and 124) was nearly equivalent to a Gcn4 deletion (Figure 5A) (Drysdale et al., 1995). Mutation of the individual aromatic residues W120 and F124 had the strongest effects, reducing the transcription of *ARG3*, *ARG5*, *and HIS4* by 2- to 3-fold. Mutation of Gcn4 L123 had a smaller effect. To test the sensitivity of the Gcn4 α-helix to mutation, proline was substituted for Gcn4 residue S122 and found to have only a minor effect on transcription, likely due to the flexibility of Gcn4 in binding to ABD1.

The cAD is highly enriched for acidic residues, with 10 of its 34 residues acidic (Figure 5B, blue). To test whether activity requires specific acidic residues or an overall negative charge, groups of 4, 5, or 9 acidic residues within the cAD were substituted with Ala. Surprisingly, these mutations had little effect on transcription from *ARG3* or *HIS4* (Figure 5A). Transcription from *ARG5* showed only modest reductions in Gcn4 constructs containing four or nine acidic residues changed to Ala, and transcription of *ARG3* was slightly elevated. Mutation of the one other acidic residue at position 103 also had no effect on transcription of any gene tested (data not shown). Similar results were observed when cells containing wild-type Gal11 were used (Figure S4B). From these results, we conclude that the acidic residues in the cAD are not required for function.

We also examined the in vivo role of ABD1 residues in the hydrophobic cleft, using a Gal11 derivative deleted for both ADB2 and ADB3 (Figure 6C; Δ277–404 + Δ418–696). Because all three activator-binding domains contribute additively to activation by Gcn4 (Herbig et al., 2010; Jedidi et al., 2010), this derivative shows only a 2-fold decrease in transcription of *ARG3* following deletion of ABD1 (Herbig et al., 2010; Jedidi et al., 2010). *ARG3* transcription decreased nearly equivalently by deletion of ABD1 or by the mutations on the floor of binding cleft W196A and A216D, both of which disrupt the folding of Gal11 (Figure 5D and data not shown). M213A, shown above to decrease the affinity for Gcn4, also decreased transcription, whereas Y220A, V170A, or the double-mutant V170A, T200A, showed no significant change in *ARG3* expression. Combined with the in vitro binding assays described earlier, these in vivo results show that Gal11 side chains within the binding cleft are not solely involved in activator recognition. Residues W196, 213, and 216 likely play a role in both stabilization of ABD1 structure and activator binding.

Gcn4 Recognizes Other Activator-Binding Domains Using a Conserved Mechanism

The Gcn4-cAD specifically binds at least two other Gal11 activator-binding domains and a domain in Taf12 (Herbig et al., 2010; Jedidi et al., 2010; Majmudar et al., 2009). To test whether Gcn4 uses a similar mechanism to bind to these other domains, we examined the HSQC spectrum of ^{15}N-Gcn4-cAD upon binding to either Gal11 residues 496–651 (ABD3) or Taf12 residues 29–259 (Figure 6). cAD chemical-shift perturbations observed upon addition of unlabeled Taf12 or ABD3 are remarkably similar to those seen with ABD1 (Figure 1B). In each case, the same Gcn4 residues undergo the largest backbone amide perturbations, although the absolute magnitudes of resonance perturbations are smaller compared to Gcn4 binding to Gal11-ABD1 (compare Figures 1C and S5). These observations indicate that the Gcn4-cAD uses a similar interface to interact with each of these domains. Therefore, the ability of Gcn4 to adopt

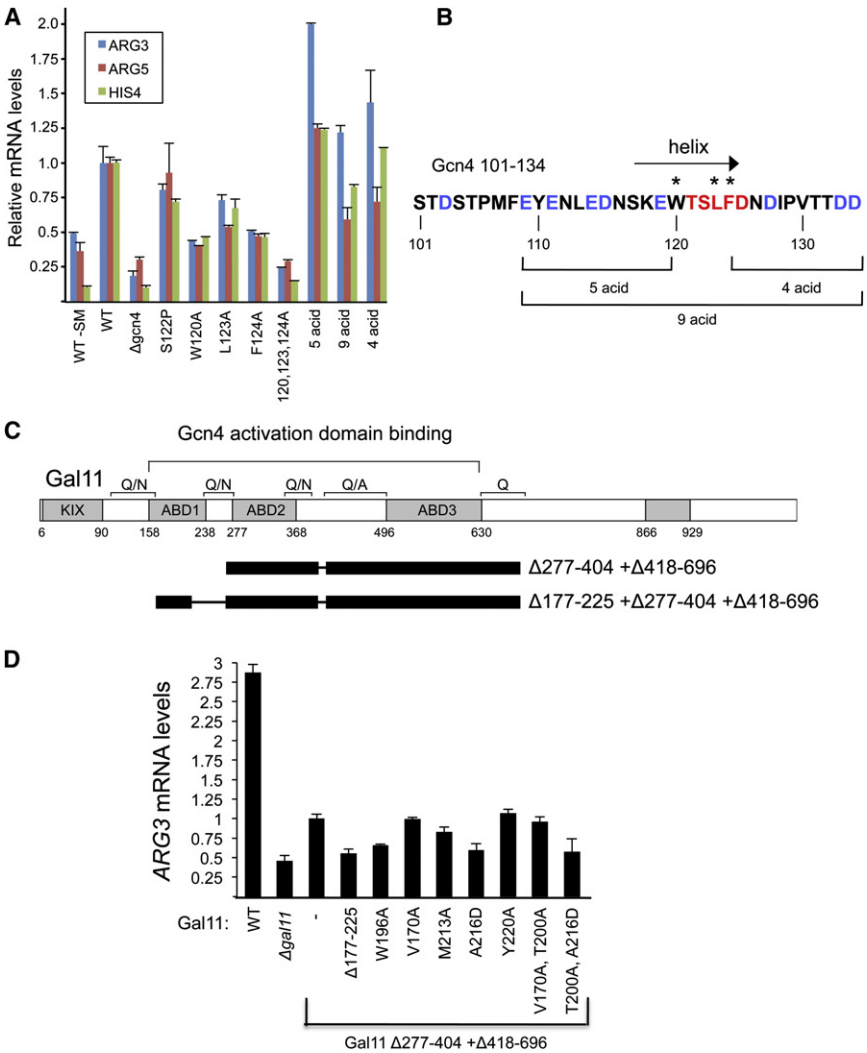

Figure 5. Effect of Mutations in the cAD-ABD1 Interface on Transcription Activation In Vivo

(A) Cells with the indicated Gcn4 mutations and Gal11 Δ418-696 were induced for 90 min with SM (sulfometuron methyl; except where noted, -SM) to induce starvation. mRNA was extracted and quantitated by RT qPCR. Error bars represent the SEM.

(B) Sequence of the cAD. Residues with the largest chemical shift perturbations (Figure 1B) are red; acidic residues outside of this region are blue. The arrow indicates the position of the α-helix formed upon binding Gal11. * indicates the position of alanine substitutions at hydrophobic residues and brackets indicate the positions of acidic residues substituted with Ala.

(C) Schematic of the Gal11 derivative used for mutagenesis of ABD1 where black bars represent regions deleted from Gal11. Conserved regions of Gal11 are shown by shaded boxes.

(D) Cell grown as in (A) and mRNA quantitated by RT qPCR. Error bars represent the SEM.

See also Figure S4.

α-helical conformation may be an element that is common to the formation of each complex.

DISCUSSION

Assembly of the transcription pre-initiation complex (PIC) relies on a number of low affinity and relatively low specificity protein-protein and protein-DNA interactions (e.g., TBP-TATA, TAF-INR, TFIIB-DNA, and Pol II-TFIIB). Even among these low affinity complexes, transcription activator/target interactions stand out as particularly enigmatic (Sigler, 1988). Critical structural elements are difficult to define because there is little sequence conservation among transcription ADs and these domains are often structurally disordered in the absence of a binding partner (Tompa and Fuxreiter, 2008). Mutational analysis can be ambiguous because multiple mutations are often required to significantly alter activator activity. In addition, a single AD may bind to multiple unrelated activator-binding domains, indicating that adaptability in the binding interface is an important structural characteristic. In cases where structures have been determined, the ADs use one or two amphipathic α-helices to form complexes with well-defined geometry. In these structures, the binding interface is composed primarily of interactions between hydrophobic residues with additional polar and/or charged contacts (Bochkareva et al., 2005; Dames et al., 2002; Di Lello et al., 2006; Langlois et al., 2008; Radhakrishnan et al., 1997; Uesugi et al., 1997; Zor et al., 2004). Importantly, polar and ionic interactions contribute to both binding specificity and the orientation of the two molecules in the complex; they also increase protein-protein affinity. In several cases, activator/coactivator binding is regulated by phosphorylation, wherein the phosphorylated residue makes specific contact with the activator-binding domain and greatly alters the affinity of interaction (Feng et al., 2009; Ferreon et al., 2009; Radhakrishnan et al., 1997). The interaction between the p53 AD and MDM2 represents one example where hydrophobic contacts predominate. Three hydrophobic residues of p53 bind in a deep hydrophobic cleft in MDM2 with high steric complementarity, forming a high-affinity, stable complex (Kussie et al., 1996). From these static structures, it is difficult to extrapolate to other systems, where unrelated activators interact with a common target protein, or to cases where a single activator binds multiple unrelated targets.

The Gcn4-cAD/Gal11-ABD1 complex shows two striking differences from previous activator-target complexes. First, the protein-protein interface is much simpler. Three Gcn4 residues, W120, L123, and F124, interact with hydrophobic residues in a shallow ABD1 cleft. Although the cAD and ABD1 have opposite electrostatic surface potentials, structural and mutational

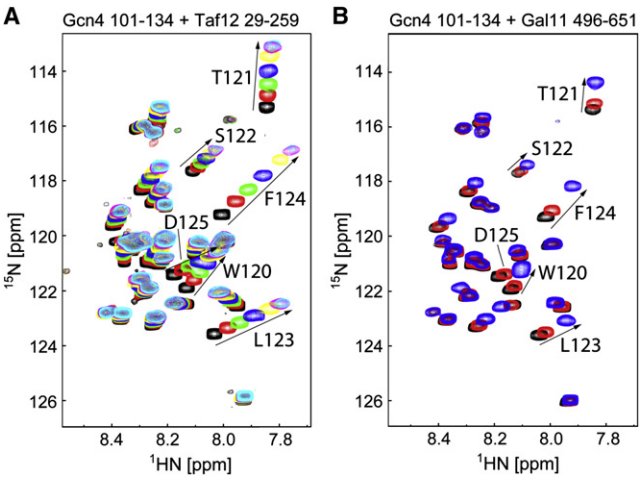

Figure 6. Gcn4 Uses Similar Mechanisms for Recognition of Taf12 and Gal11 ABD3

(A) ^{1}H,^{15}N-HSQC spectra of 0.3 mM ^{15}N-labeled Gcn4 (101-134) in the absence of (black) and presence of 0.125 (red), 0.25 (green), 0.5 (blue), 1 (yellow), 2 (magenta), or 3 equivalents (cyan) of Taf12 (29-259).

(B) ^{1}H,^{15}N-HSQC spectra of 0.3 mM ^{15}N-labeled Gcn4 (101-134) in the absence of (black) and presence of 0.1 (red) or 0.5 equivalents (blue) of Gal11 (496-651). In each spectrum, amides with the largest chemical shift perturbations (residues 120-125) are labeled and highlighted by arrows. A complete titration could not be performed due to the limited solubility of ABD3.

See also Figure S4.

analysis demonstrates that there are no specific polar or ionic interactions at the interface. This likely contributes to the second major difference from previous activator-coactivator structures: the cAD helix binds to ABD1 in multiple orientations. These properties indicate that the Gcn4-Gal11 complex is an example of a fuzzy complex in which the protein interface cannot be described by a single conformational state (see Tompa and Fuxreiter, 2008 and references therein). Fuzziness has been proposed as functionally important by providing adaptability and reversibility to protein-protein interactions, consistent with the biological function of many ADs.

Wild-type Gcn4 functionally interacts with wild-type Gal11 by binding three low-affinity activator-binding sites rather than interacting through a single high affinity, high-specificity site (Herbig et al., 2010). Our NMR results show that this binding is in fast exchange on the NMR time scale, suggesting that Gcn4 can rapidly sample multiple Gal11 activator-binding domains as a mechanism to recruit Mediator to the enhancer/promoter region. This model explains why the Gal11 activator-binding domains act additively to increase activated transcription and why multimerization of transcription factor DNA binding sites often greatly stimulates transcription. These results would not be expected if activators have a single high-affinity, high-specificity target with a slow dissociation rate.

Unexpectedly, we found that acidic residues within the cAD are not essential for function. Because Gal11 has a net overall positive charge, we expected that nonspecific electrostatic interactions would contribute to long-range attractions between Gcn4-Gal11 (Shoemaker et al., 2000). It is possible that the electrostatic properties of Gcn4-ADs and Gal11-ABDs act as a screen to prevent unwanted interactions with proteins that have a suitable hydrophobic interface but also have the wrong surface potential. In either case, our mutagenesis results emphasize the lack of highly specific electrostatic interactions in the Gcn4-cAD/Gal11-ABD1 complex, consistent with our model for multiple modes of Gcn4-Gal11 binding.

To activate transcription, Gcn4 must also interact with other coactivator subunits unrelated to Gal11. Our results show that the cAD uses the same key residues to interact with Gal11-ABD3 and the activator-binding domain of Taf12. Given the simple nature of the Gcn4/Gal11 interface, these other activator-binding domains likely bind Gcn4 using a similar mechanism. The low affinity and specificity of Gcn4/target interactions seem to require only a simple protein-protein interface where the activator can readily adapt to fit a fairly generic hydrophobic binding cleft.

What, then, defines the requirements for a minimal AD? Gcn4 consists of an inherently disordered polypeptide, with a segment that is able to adopt a helical fold when bound to its targets. This helical segment has hydrophobic residues at positions i, i +3, i +4 (residues 120, 123, and 124) on the same face of the helix. This pattern has been noted previously in several activators (Chi et al., 2005; Uesugi et al., 1997) and includes the LXXLL interaction motif (Darimont et al., 1998; Nolte et al., 1998). Within Gcn4, the aromatic residues at positions 120 and 124 are the most important for activity because these two residues define the minimal pattern for Gcn4 activator function. Sequence motifs vary among well-characterized activators. The acidic activators VP16, p53, and EKLF (Chi et al., 2005; Mas et al., 2011; Uesugi et al., 1997) all contain sequences that match the motif described for Gcn4-cAD, where at least one of these hydrophobic residues is functionally important (Cress and Triezenberg, 1991; Lin et al., 1994; Mas et al., 2011). In contrast, Gal4 has two overlapping matches to this pattern; however, mutagenesis of nearly every residue within the Gal4 AD has not revealed any one residue critical for activator function (Ansari et al., 1998). Although the Gcn4-N-terminal AD contains two matches to this pattern, functional studies define this AD as nearly 100 residues in length, suggesting that it does not use the minimal motif (Jackson et al., 1996). Future studies that seek to precisely define the minimal activator motif and examine the mechanism of more complex activators will be highly informative for defining different classes of activators and increasing the understanding of the diverse mechanisms used in eukaryotic transcriptional regulation.

EXPERIMENTAL PROCEDURES

See also Supplemental Experimental Procedures.

NMR Experiments and Resonance Assignments

NMR experiments were performed at 25°C on a Bruker 500 MHz AVANCE or Varian INOVA spectrometer (600 MHz, 800 MHz, or 900 MHz instruments located at Pacific Northwest National Laboratories). Data were processed and analyzed using NMRPipe (Delaglio et al., 1995) and NMRView (Johnson and Blevins, 1994). NMR samples for Gal11-ABD1 structure determination consisted of 1.2 mM [^{13}C,^{15}N]-Gal11-ABD1 plus 2.4 mM unlabeled Gcn4-cAD in NMR buffer with 10% or 99% D_2O. Likewise, 1.2 mM [^{13}C,^{15}N]-Gcn4-cAD with and without 2.4 mM unlabeled Gal11-ABD1 were

used for the assignment of the backbone and side-chain resonances of free and bound Gcn4. Assignment of backbone and side-chain resonances was accomplished by analysis of standard triple-resonance experiments (Sattler et al., 1999, see also Supplemental Experimental Procedures). Mixing times for NOESY-based experiments were 140 ms.

Structure Calculations and Modeling

Distance restraints for calculation of the Gal11-ABD1 domain were obtained by manual inspection of 3D-NOESY experiments. Only unambiguous cross-peaks with symmetry-related resonances were used; interacting atoms were binned based on observed NOE intensities and used to generate distance constraints. Constraints involving side chains of residues found to be involved in intermolecular interactions were excluded. Dihedral backbone angle-restraints for Gal11 were predicted from backbone assignments and generated using TALOS (Cornilescu et al., 1999). Only dihedral angle restraints with good fits were included. These constraints were used as input for structure calculations in CNS 1.3. (Brünger et al., 1998).

The 20 lowest energy structures were used in calculations to model the complex formed with Gcn4-cAD. Edited-filtered NOESY experiments were used to define interacting Gal11 and Gcn4 residues. These data were then used to generate ambiguous interaction restraints to model the complex using the docking program HADDOCK (Dominguez et al., 2003). The resulting models were compared with the results of spin-labeling experiments (see below) to identify structures that most closely reflect experimental observations.

Paramagnetic Relaxation Enhancement Experiments with Spin-Labeled Gcn4

Single-cysteine mutants of Gcn4 (101-134) were prepared through site-directed mutagenesis (S104C, S117C, N126C, and D133C) and modified with 4-(2-Iodoacetamido)-TEMPO. To measure paramagnetic relaxation enhancement, we added 0.6 mM spin-labeled Gcn4 mutant-protein to 0.3 mM ^{15}N-labeled Gal11 (158-238). ^{1}H,^{15}N-HSQC spectra were collected in the absence and presence of 3 mM ascorbic acid (to reduce the paramagnetic nitroxide). The intensity of each backbone amide resonance was measured to calculate the ratio of the intensity in the absence of ascorbic acid versus the intensity in the presence of ascorbic acid.

ACCESSION NUMBERS

The BioMagResBank accession number for the chemical shift assignments for Gcn4-bound Gal11 and Gal11-bound Gcn4 is 16488.

Models of the Gcn4-cAD complex have been deposited in the Protein Bank under ID code 2KO4.

SUPPLEMENTAL INFORMATION

Supplemental Information includes Supplemental Experimental Procedures and Figures S1–S5 and can be found with this article online at doi:10.1016/j.molcel.2011.11.008.

ACKNOWLEDGMENTS

We thank Barry Stoddard and members of the Hahn and Klevit laboratories for comments and suggestions during the course of this work and Nadia Kulshina for help with ITC experiments. NMR experiments were performed, in part, in the Environmental Molecular Sciences Laboratories at the Pacific Northwest National Laboratories. D.B. is an HHMI investigator. This work was funded by NIH grant GM075114 to S.H. and a Boehringer Ingelheim Fonds Ph.D. Scholarship to C.C.H.; R.E.K. and P.S.B. are supported by NIH R01 GM088055 and EY017370.

Received: June 1, 2010
Revised: July 19, 2011
Accepted: October 7, 2011
Published: December 22, 2011

REFERENCES

Ansari, A.Z., Reece, R.J., and Ptashne, M. (1998). A transcriptional activating region with two contrasting modes of protein interaction. Proc. Natl. Acad. Sci. USA *95*, 13543–13548.

Bochkareva, E., Kaustov, L., Ayed, A., Yi, G.S., Lu, Y., Pineda-Lucena, A., Liao, J.C., Okorokov, A.L., Milner, J., Arrowsmith, C.H., and Bochkarev, A. (2005). Single-stranded DNA mimicry in the p53 transactivation domain interaction with replication protein A. Proc. Natl. Acad. Sci. USA *102*, 15412–15417.

Brown, C.E., Howe, L., Sousa, K., Alley, S.C., Carrozza, M.J., Tan, S., and Workman, J.L. (2001). Recruitment of HAT complexes by direct activator interactions with the ATM-related Tra1 subunit. Science *292*, 2333–2337.

Brünger, A.T., Adams, P.D., Clore, G.M., DeLano, W.L., Gros, P., Grosse-Kunstleve, R.W., Jiang, J.S., Kuszewski, J., Nilges, M., Pannu, N.S., et al. (1998). Crystallography & NMR system: A new software suite for macromolecular structure determination. Acta Crystallogr. D Biol. Crystallogr. *54*, 905–921.

Campbell, A.P., and Sykes, B.D. (1993). The two-dimensional transferred nuclear Overhauser effect: theory and practice. Annu. Rev. Biophys. Biomol. Struct. *22*, 99–122.

Chi, S.W., Lee, S.H., Kim, D.H., Ahn, M.J., Kim, J.S., Woo, J.Y., Torizawa, T., Kainosho, M., and Han, K.H. (2005). Structural details on mdm2-p53 interaction. J. Biol. Chem. *280*, 38795–38802.

Cornilescu, G., Delaglio, F., and Bax, A. (1999). Protein backbone angle restraints from searching a database for chemical shift and sequence homology. J. Biomol. NMR *13*, 289–302.

Cress, W.D., and Triezenberg, S.J. (1991). Critical structural elements of the VP16 transcriptional activation domain. Science *251*, 87–90.

Dames, S.A., Martinez-Yamout, M., De Guzman, R.N., Dyson, H.J., and Wright, P.E. (2002). Structural basis for Hif-1 alpha /CBP recognition in the cellular hypoxic response. Proc. Natl. Acad. Sci. USA *99*, 5271–5276.

Darimont, B.D., Wagner, R.L., Apriletti, J.W., Stallcup, M.R., Kushner, P.J., Baxter, J.D., Fletterick, R.J., and Yamamoto, K.R. (1998). Structure and specificity of nuclear receptor-coactivator interactions. Genes Dev. *12*, 3343–3356.

Delaglio, F., Grzesiek, S., Vuister, G.W., Zhu, G., Pfeifer, J., and Bax, A. (1995). NMRPipe: a multidimensional spectral processing system based on UNIX pipes. J. Biomol. NMR *6*, 277–293.

Di Lello, P., Jenkins, L.M., Jones, T.N., Nguyen, B.D., Hara, T., Yamaguchi, H., Dikeakos, J.D., Appella, E., Legault, P., and Omichinski, J.G. (2006). Structure of the Tfb1/p53 complex: Insights into the interaction between the p62/Tfb1 subunit of TFIIH and the activation domain of p53. Mol. Cell *22*, 731–740.

Dominguez, C., Boelens, R., and Bonvin, A.M. (2003). HADDOCK: a protein-protein docking approach based on biochemical or biophysical information. J. Am. Chem. Soc. *125*, 1731–1737.

Drysdale, C.M., Dueñas, E., Jackson, B.M., Reusser, U., Braus, G.H., and Hinnebusch, A.G. (1995). The transcriptional activator GCN4 contains multiple activation domains that are critically dependent on hydrophobic amino acids. Mol. Cell. Biol. *15*, 1220–1233.

Dunker, A.K., Lawson, J.D., Brown, C.J., Williams, R.M., Romero, P., Oh, J.S., Oldfield, C.J., Campen, A.M., Ratliff, C.M., Hipps, K.W., et al. (2001). Intrinsically disordered protein. J. Mol. Graph. Model. *19*, 26–59.

Dyson, H.J., and Wright, P.E. (2005). Intrinsically unstructured proteins and their functions. Nat. Rev. Mol. Cell Biol. *6*, 197–208.

Feng, H., Jenkins, L.M., Durell, S.R., Hayashi, R., Mazur, S.J., Cherry, S., Tropea, J.E., Miller, M., Wlodawer, A., Appella, E., and Bai, Y. (2009). Structural basis for p300 Taz2-p53 TAD1 binding and modulation by phosphorylation. Structure *17*, 202–210.

Ferreon, J.C., Lee, C.W., Arai, M., Martinez-Yamout, M.A., Dyson, H.J., and Wright, P.E. (2009). Cooperative regulation of p53 by modulation of ternary complex formation with CBP/p300 and HDM2. Proc. Natl. Acad. Sci. USA *106*, 6591–6596.

Fishburn, J., Mohibullah, N., and Hahn, S. (2005). Function of a eukaryotic transcription activator during the transcription cycle. Mol. Cell *18*, 369–378.

Freedman, S.J., Sun, Z.Y., Poy, F., Kung, A.L., Livingston, D.M., Wagner, G., and Eck, M.J. (2002). Structural basis for recruitment of CBP/p300 by hypoxia-inducible factor-1 alpha. Proc. Natl. Acad. Sci. USA *99*, 5367–5372.

Freedman, S.J., Sun, Z.Y., Kung, A.L., France, D.S., Wagner, G., and Eck, M.J. (2003). Structural basis for negative regulation of hypoxia-inducible factor-1alpha by CITED2. Nat. Struct. Biol. *10*, 504–512.

Ge, K., Guermah, M., Yuan, C.X., Ito, M., Wallberg, A.E., Spiegelman, B.M., and Roeder, R.G. (2002). Transcription coactivator TRAP220 is required for PPAR gamma 2-stimulated adipogenesis. Nature *417*, 563–567.

Green, M.R. (2005). Eukaryotic transcription activation: right on target. Mol. Cell *18*, 399–402.

Herbig, E., Warfield, L., Fish, L., Fishburn, J., Knutson, B.A., Moorefield, B., Pacheco, D., and Hahn, S. (2010). Mechanism of Mediator recruitment by tandem Gcn4 activation domains and three Gal11 activator-binding domains. Mol. Cell. Biol. *30*, 2376–2390.

Hinnebusch, A.G. (2005). Translational regulation of GCN4 and the general amino acid control of yeast. Annu. Rev. Microbiol. *59*, 407–450.

Holm, L., Kääriäinen, S., Rosenström, P., and Schenkel, A. (2008). Searching protein structure databases with DaliLite v.3. Bioinformatics *24*, 2780–2781.

Hope, I.A., Mahadevan, S., and Struhl, K. (1988). Structural and functional characterization of the short acidic transcriptional activation region of yeast GCN4 protein. Nature *333*, 635–640.

Huth, J.R., Bewley, C.A., Jackson, B.M., Hinnebusch, A.G., Clore, G.M., and Gronenborn, A.M. (1997). Design of an expression system for detecting folded protein domains and mapping macromolecular interactions by NMR. Protein Sci. *6*, 2359–2364.

Irniger, S., and Braus, G.H. (2003). Controlling transcription by destruction: the regulation of yeast Gcn4p stability. Curr. Genet. *44*, 8–18.

Jackson, B.M., Drysdale, C.M., Natarajan, K., and Hinnebusch, A.G. (1996). Identification of seven hydrophobic clusters in GCN4 making redundant contributions to transcriptional activation. Mol. Cell. Biol. *16*, 5557–5571.

Jedidi, I., Zhang, F., Qiu, H., Stahl, S.J., Palmer, I., Kaufman, J.D., Nadaud, P.S., Mukherjee, S., Wingfield, P.T., Jaroniec, C.P., and Hinnebusch, A.G. (2010). Activator Gcn4 employs multiple segments of Med15/Gal11, including the KIX domain, to recruit mediator to target genes in vivo. J. Biol. Chem. *285*, 2438–2455.

Johnson, B.A., and Blevins, R.A. (1994). NMR VIEW: a computer program for the visualization and analysis of NMR data. J. Biomol. NMR *4*, 603–614.

Kussie, P.H., Gorina, S., Marechal, V., Elenbaas, B., Moreau, J., Levine, A.J., and Pavletich, N.P. (1996). Structure of the MDM2 oncoprotein bound to the p53 tumor suppressor transactivation domain. Science *274*, 948–953.

Langlois, C., Mas, C., Di Lello, P., Jenkins, L.M., Legault, P., and Omichinski, J.G. (2008). NMR structure of the complex between the Tfb1 subunit of TFIIH and the activation domain of VP16: structural similarities between VP16 and p53. J. Am. Chem. Soc. *130*, 10596–10604.

Lin, J., Chen, J., Elenbaas, B., and Levine, A.J. (1994). Several hydrophobic amino acids in the p53 amino-terminal domain are required for transcriptional activation, binding to mdm-2 and the adenovirus 5 E1B 55-kD protein. Genes Dev. *8*, 1235–1246.

Ma, J., and Ptashne, M. (1987). Deletion analysis of GAL4 defines two transcriptional activating segments. Cell *48*, 847–853.

Majmudar, C.Y., Wang, B., Lum, J.K., Håkansson, K., and Mapp, A.K. (2009). A high-resolution interaction map of three transcriptional activation domains with a key coactivator from photo-cross-linking and multiplexed mass spectrometry. Angew. Chem. Int. Ed. Engl. *48*, 7021–7024.

Marsh, J.A., Singh, V.K., Jia, Z., and Forman-Kay, J.D. (2006). Sensitivity of secondary structure propensities to sequence differences between alpha- and gamma-synuclein: implications for fibrillation. Protein Sci. *15*, 2795–2804.

Martchenko, M., Levitin, A., and Whiteway, M. (2007). Transcriptional activation domains of the Candida albicans Gcn4p and Gal4p homologs. Eukaryot. Cell *6*, 291–301.

Mas, C., Lussier-Price, M., Soni, S., Morse, T., Arseneault, G., Di Lello, P., Lafrance-Vanasse, J., Bieker, J.J., and Omichinski, J.G. (2011). Structural and functional characterization of an atypical activation domain in erythroid Kruppel-like factor (EKLF). Proc. Natl. Acad. Sci. USA *108*, 10484–10489.

Mittler, G., Stühler, T., Santolin, L., Uhlmann, T., Kremmer, E., Lottspeich, F., Berti, L., and Meisterernst, M. (2003). A novel docking site on Mediator is critical for activation by VP16 in mammalian cells. EMBO J. *22*, 6494–6504.

Nolte, R.T., Wisely, G.B., Westin, S., Cobb, J.E., Lambert, M.H., Kurokawa, R., Rosenfeld, M.G., Willson, T.M., Glass, C.K., and Milburn, M.V. (1998). Ligand binding and co-activator assembly of the peroxisome proliferator-activated receptor-gamma. Nature *395*, 137–143.

Park, J.M., Kim, H.S., Han, S.J., Hwang, M.S., Lee, Y.C., and Kim, Y.J. (2000). In vivo requirement of activator-specific binding targets of mediator. Mol. Cell. Biol. *20*, 8709–8719.

Prochasson, P., Neely, K.E., Hassan, A.H., Li, B., and Workman, J.L. (2003). Targeting activity is required for SWI/SNF function in vivo and is accomplished through two partially redundant activator-interaction domains. Mol. Cell *12*, 983–990.

Ptashne, M., and Gann, A. (2002). Genes & Signals (Cold Spring Harbor, NY: Cold Spring Harbor Laboratory Press).

Radhakrishnan, I., Pérez-Alvarado, G.C., Parker, D., Dyson, H.J., Montminy, M.R., and Wright, P.E. (1997). Solution structure of the KIX domain of CBP bound to the transactivation domain of CREB: a model for activator:coactivator interactions. Cell *91*, 741–752.

Reeves, W.M., and Hahn, S. (2005). Targets of the Gal4 transcription activator in functional transcription complexes. Mol. Cell. Biol. *25*, 9092–9102.

Sattler, M., Schleucher, J., and Griesinger, C. (1999). Heteronuclear multidimensional NMR experiments for the structure determination of proteins in solution employing pulsed field gradients. Prog NMR Spectrosc. *34*, 93–158.

Shen, Y., Lange, O., Delaglio, F., Rossi, P., Aramini, J.M., Liu, G., Eletsky, A., Wu, Y., Singarapu, K.K., Lemak, A., et al. (2008). Consistent blind protein structure generation from NMR chemical shift data. Proc. Natl. Acad. Sci. USA *105*, 4685–4690.

Shen, Y., Vernon, R., Baker, D., and Bax, A. (2009). De novo protein structure generation from incomplete chemical shift assignments. J. Biomol. NMR *43*, 63–78.

Shoemaker, B.A., Portman, J.J., and Wolynes, P.G. (2000). Speeding molecular recognition by using the folding funnel: the fly-casting mechanism. Proc. Natl. Acad. Sci. USA *97*, 8868–8873.

Sigler, P.B. (1988). Transcriptional activation. Acid blobs and negative noodles. Nature *333*, 210–212.

Stevens, J.L., Cantin, G.T., Wang, G., Shevchenko, A., Shevchenko, A., and Berk, A.J. (2002). Transcription control by E1A and MAP kinase pathway via Sur2 mediator subunit. Science *296*, 755–758.

Suhrer, S.J., Wiederstein, M., Gruber, M., and Sippl, M.J. (2009). COPS–a novel workbench for explorations in fold space. Nucleic Acids Res. *37*, W539–W544.

Swanson, M.J., Qiu, H., Sumibcay, L., Krueger, A., Kim, S.J., Natarajan, K., Yoon, S., and Hinnebusch, A.G. (2003). A multiplicity of coactivators is required by Gcn4p at individual promoters in vivo. Mol. Cell. Biol. *23*, 2800–2820.

Sykes, B.D. (1993). Determination of the conformations of bound peptides using NMR-transferred nOe techniques. Curr. Opin. Biotechnol. *4*, 392–396.

Tompa, P., and Fuxreiter, M. (2008). Fuzzy complexes: polymorphism and structural disorder in protein-protein interactions. Trends Biochem. Sci. *33*, 2–8.

Uesugi, M., Nyanguile, O., Lu, H., Levine, A.J., and Verdine, G.L. (1997). Induced alpha helix in the VP16 activation domain upon binding to a human TAF. Science *277*, 1310–1313.

Wishart, D.S., Sykes, B.D., and Richards, F.M. (1991). Relationship between nuclear magnetic resonance chemical shift and protein secondary structure. J. Mol. Biol. *222*, 311–333.

Yang, F., DeBeaumont, R., Zhou, S., and Näär, A.M. (2004). The activator-recruited cofactor/Mediator coactivator subunit ARC92 is a functionally important target of the VP16 transcriptional activator. Proc. Natl. Acad. Sci. USA *101*, 2339–2344.

Yoon, S., Qiu, H., Swanson, M.J., and Hinnebusch, A.G. (2003). Recruitment of SWI/SNF by Gcn4p does not require Snf2p or Gcn5p but depends strongly on SWI/SNF integrity, SRB mediator, and SAGA. Mol. Cell. Biol. *23*, 8829–8845.

Zor, T., De Guzman, R.N., Dyson, H.J., and Wright, P.E. (2004). Solution structure of the KIX domain of CBP bound to the transactivation domain of c-Myb. J. Mol. Biol. *337*, 521–534.